Dark Currents in Superconducting Radio-Frequency Cavities

George Hang

Department of Physics and Astronomy,

Swarthmore College, Swarthmore, PA, 19081

(Dated: 10 August 2005)

Computer simulation of multpacting in the ILC reentrant cavity reveals a potential multipacting barrier at 52.5 MV/m peak surface electric field for the multi-cell cavities and a barrier at 55 MV/m peak surface electric field for the single-cell test cavity. Computer simulation of field emission in the ERL two-cell injector cavity reveals a general trend that more field emitted electrons tend to penetrate the beam tube with increasing peak surface electric field ranging from 10 to 30 MV/m. Plausible scenarios of field emission induced multpacting and a temporal focusing effect of field emission were identified. A predicted maximum total power output of a single ERL cavity emitter with an effective area of 10^{-8}cm^2 and an enhancement factor of 200 is on the order of 10 kW.

I. INTERNATIONAL LINEAR COLLIDER REENTRANT CAVITY

Previous work on optimization of high beta cavities have lead to the reentrant cavity design for the International Linear Collider.[1] Pending vertical and horizontal testing, this design benefits from an examination of potential multipactors using a computer simulation code MultiPac 2.1.

Multipacting is the phenomenon where electrons emitted from the surface bombard back at the surface to generate more electrons and cause an avalanche effect that consumes available radio-frequency (RF) power. Early accelerating cavities suffered from single point multipacting where the emitted electrons follow a trajectory such that they return to a point close to the originial emission site in an intergral number of RF cycles after emission and generate more electrons than before. The elliptic design overcomes single point multipactors, yet suffers from two point multipacting, which is when the emitted electrons bombard the cavity at a point different from the original emission point and the secondary electrons bombard the original emission point, creating an oscillating electron current effect that similarly consumes available RF power.

The simulation code Multipac uses an enhanced counter function to gauge the availability and intesnity of multipacting as the peak surface electric field, which corresponds to the accelerating gradient, changes. An indicator for multipacting is denoted by an enhanced counter function greater than unity. The energy of an emitted electron varies mostly between 2 eV and 5 eV. Therefore, simulations were performed at these two extremes.

For an assumed 2 eV energy for an emitted electron, Fig. 1 and 2 show the enhanced counter function and the trajectories, respectively, and reveal a potential multipacting barrier centered around 52.5 MV/m peak surface electric field with a range approximately 3 MV/m and average impact energy of 35 eV. For an assumed 5 eV energy for an emitted electron, a multipacting barrier is predicted to exist around 52.5 MV/m peak surface electric field, same as the 2 eV case, with a greater range approximately 13 MV/m as shown in Fig. 3 and a higher average impact energy of 82.6 eV as shown in Fig. 4.
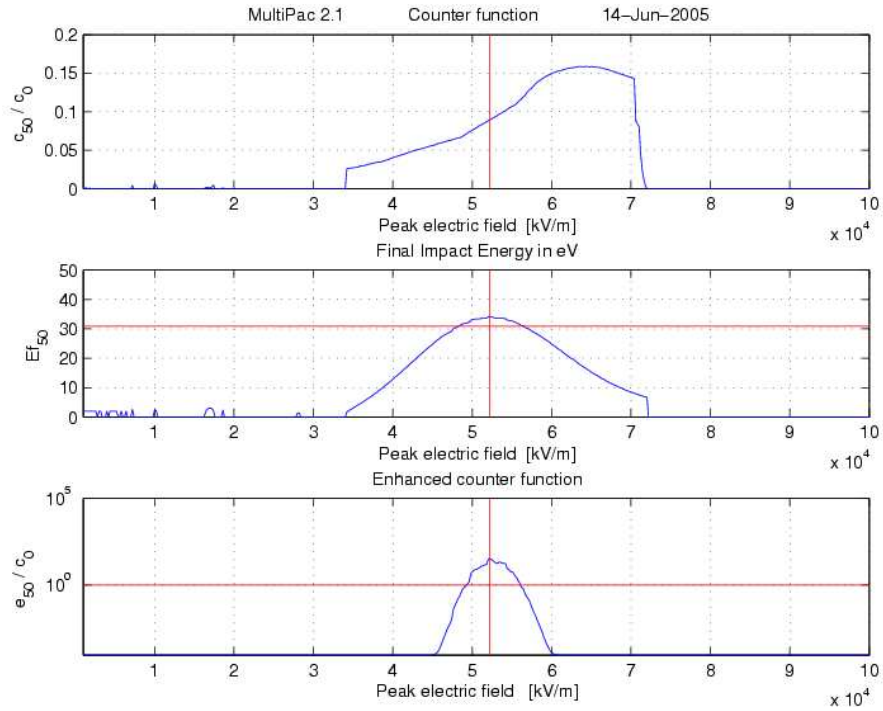
FIG. 1: Multi-cell Cavity Counter Results at 2 eV — A reasonable lower bound for emitted electron energy is 2 eV.
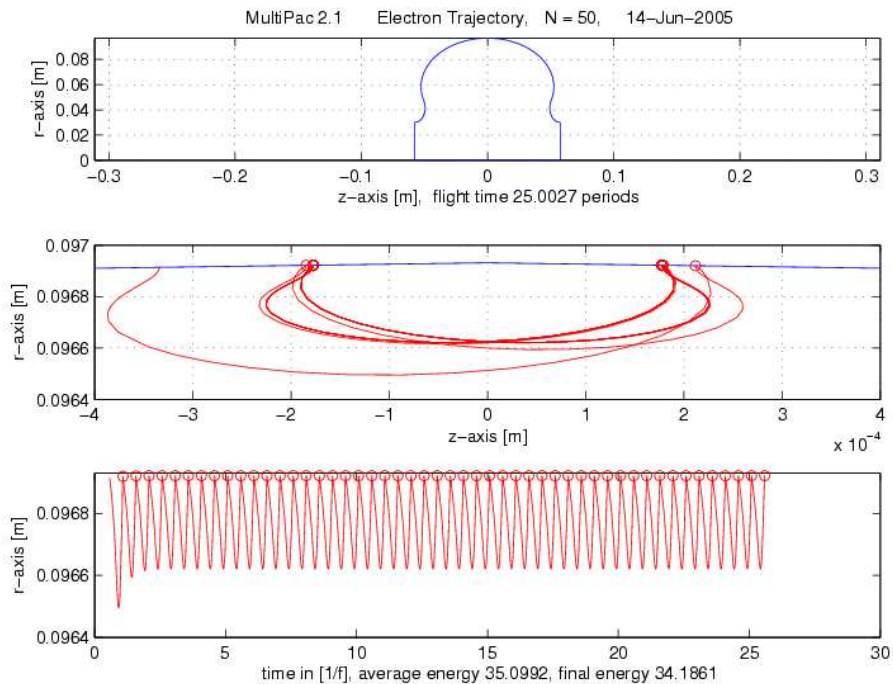

FIG. 2: Multi-cell Cavity Trajectory Map at 2 eV — The results suggest that when the emitted electron energy is on the lower end, then the average impact energy is low. Therefore, this barrier will probably not be a limiting barrier.
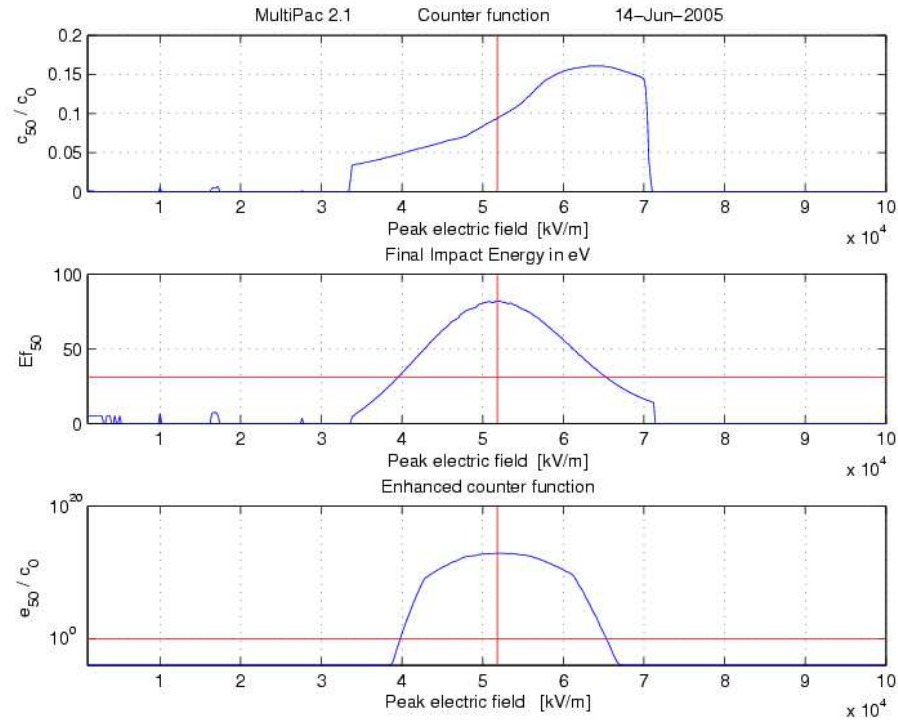
FIG. 3: Multi-cell Cavity Counter Results at 5 eV — A reasonable upper bound for emitted electron energy is 5 eV.
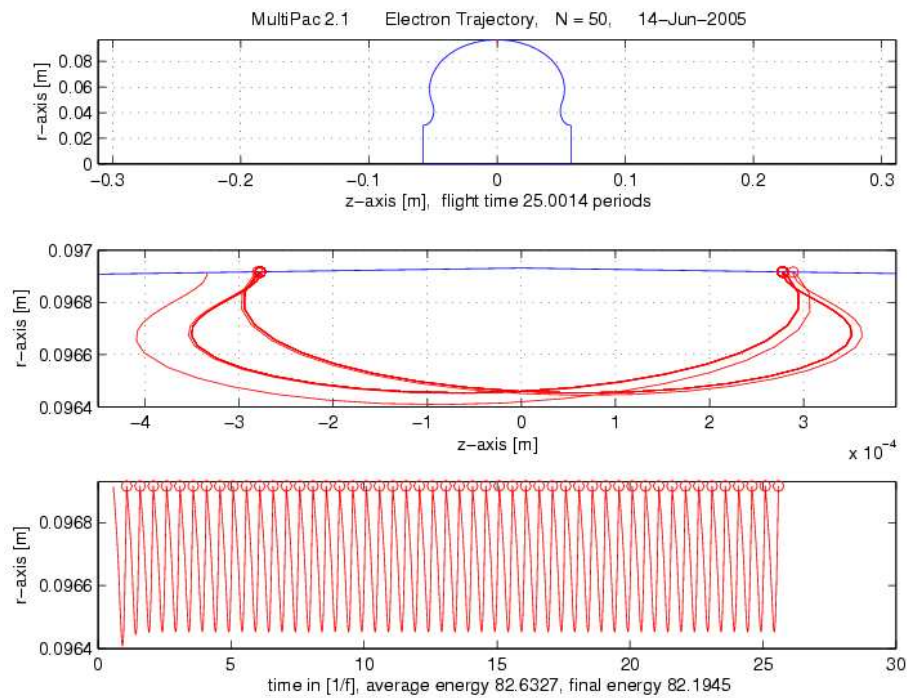

FIG. 4: Multi-cell Cavity Trajectory Map at 5 eV — The results show that multipacting may be potentially a limiting factor in cases where the emitted electron energy is higher.

Similar simulations were performed for the single cell testing cavity, which reveal a potential multipacting barrier centered around 55 MV/m peak surface electric field with a range approximately 3 MV/m and average impact energy of 35.6 eV for the 2 eV case as shown in Fig. 5 and 6. A potential multipacting barrier was identified around 55 MV/m peak surface electric field with a range around 13 MV/m and an average impact energy of 83.9 eV for the 5 eV case, shown in Fig. 7 and 8.
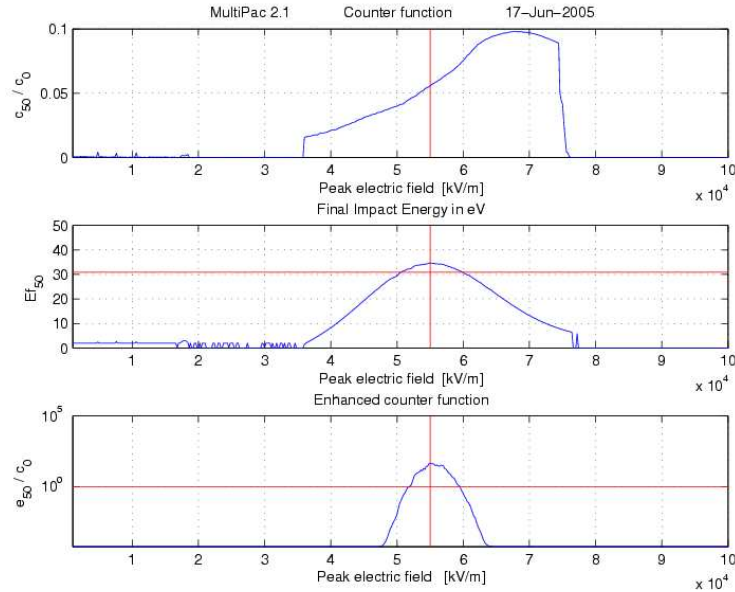

FIG. 5: Single-cell Cavity Counter Results at 2 eV — The different boundary conditions at the irises shifts the peak of the enhanced counter function in the single cell case.
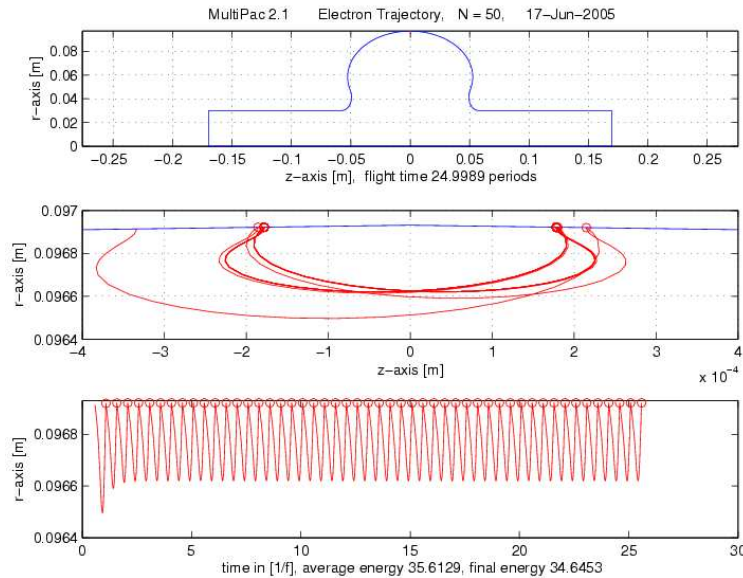

FIG. 6: Single-cell Cavity Trajectory Map at 2 eV — As suggested in Fig. 2, the lower impact energy indicates the multipacting is not an issue.
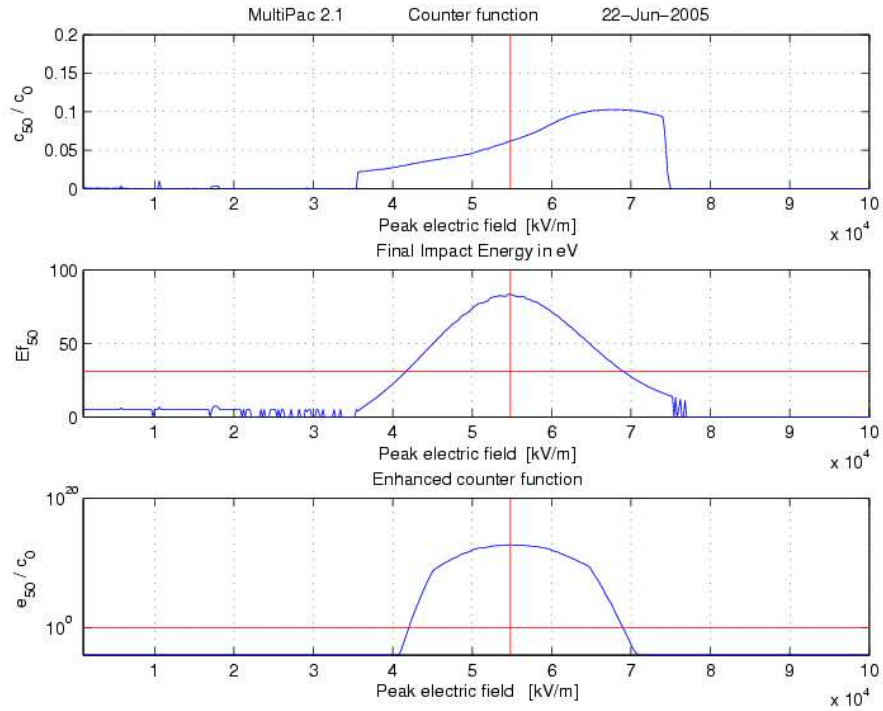
FIG. 7: Single-cell Cavity Counter Results at 5 eV — Results from both the single-cell and multi-cell cavity suggest that the peak of the enhanced counter function does not depend on emitted electron energy.
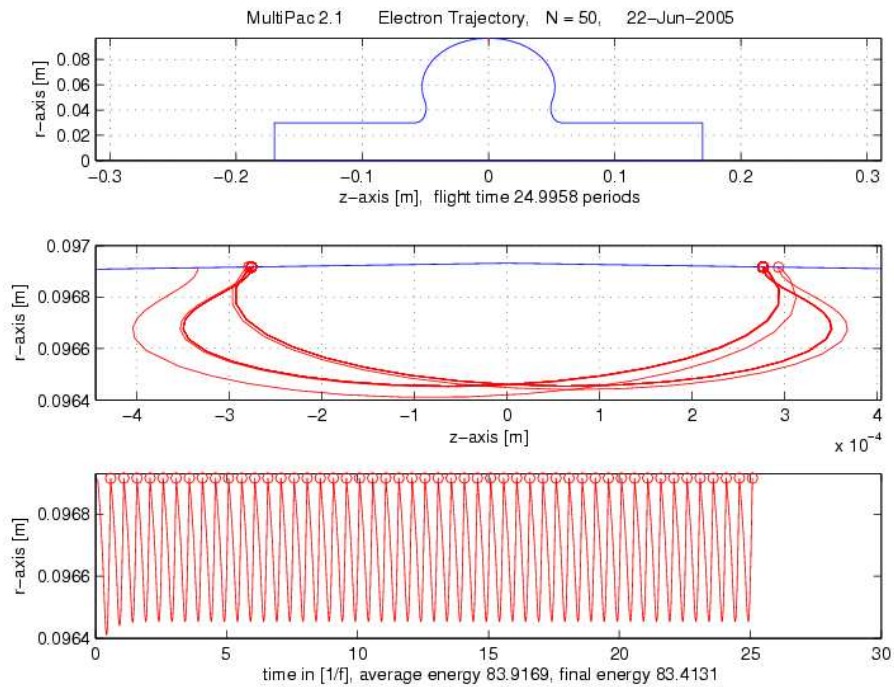

FIG. 8: Single-cell Cavity Trajectory Map at 5 eV — The higher impact energy is an issue, as suggested in Fig. 4.

While the simulation results above predict a multipactor, the barrier may be surpassable. Previous work have shown that similar low energy multipacting barriers in other superconducting RF (SRF) cavities have been surpassed by using various processing techniques including conditioning,[2] which uses the multipacting bombardment to clean the cavity surface and shift the secondary emission curve below unity as shown in Fig. 9.[3] However, in cases of extreme roughness or uncleanliness, conditioning may not suffice and additional cleaning procedures are required.
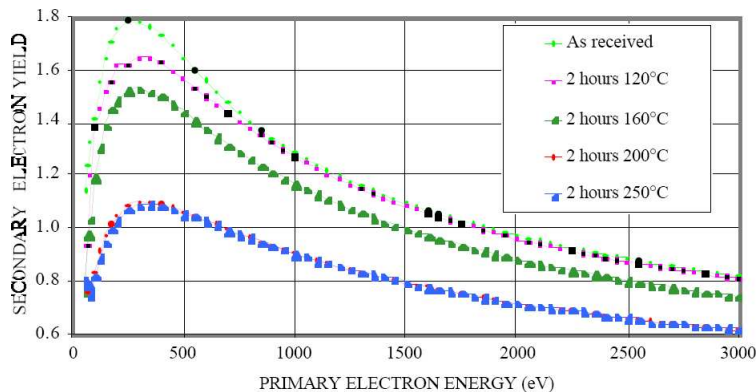

FIG. 9: Secondary Curve Shift — The graph shows the effects of baking, which is effectively the same as that of conditioning. In baking the energy source is thermionic and in conditioning the energy is from the bombarding electrons.

II. CORNELL ENERGY RECOVERY LINEAR ACCELERATOR INJECTOR CAVITY

Previous work on the Cornell Energy Recovery LinAc (ERL) have led to the design of a dipole-mode-free and kick-free two-cell injector cavity [4] that is currently under construction. This investigation seeks to assess possible field emission related damage and complications with an emphasis on secondary electrons generated by the bombardment of the cavity and beam tube higher-order mode (HOM) absorber surfaces.

The simulation was performed by a modified version of the computer simulation code Multip that tracks trajectories for longer periods of time. The electromagnetic field generated by solving a slightly simplifed cavity geometry, created by a pre-processor Shapes, with the computer code SuperLANS that uses a finite element method and has a higher accuracy in eigenvalue solving than comparable codes.[5] Emitters were seeded at 0.05 cm intervals about the irises for a range approximately equal to that the radius of curvature at every $\frac{1}{100}$ of an RF period, and the electron trajectories were tracked for a extended periods of time up to 500 RF periods using a fourth order Runga-Kutta integration.

Simulation of field emission was performed in accordance with the Fowler-Nordheim field emission theory with enhancement factor. The emitted current is determed using Eq. 1.[6]

$$I_{FN} = \frac{e^3}{8\pi h} \frac{A \left| \beta \vec{E} \right|^2}{\phi \left(t(\eta) \right)^2} \exp\left(-\frac{8\pi \sqrt{2m\phi^3} v(\eta)}{3he \left| \beta \vec{E} \right|} \right) \tag{1}$$

where e is the electron charge, m is the electron mass, h is Planck's constant, ϕ is the work function of the cavity surface, $\vec{E}$ the instantaneous surface electric field at the emitter location, η is defined by Eq. 2

$$\eta = \sqrt{\frac{e^3 \left|\beta \vec{E}\right|}{4\pi\epsilon_0 \phi^2}} \tag{2}$$

and ϵ_0 is the permittivity of free space. The function $v(\eta)$ and $t(\eta)$ can be expressed in terms of complete elliptic integrals as given by Murphy and Good as follows: [7]

For $\eta < 1$, then

$$v(\eta) = \sqrt{1+\eta}\left[E\left(\sqrt{\frac{1-\eta}{1+\eta}}\right) - \eta K\left(\sqrt{\frac{1-\eta}{1+\eta}}\right)\right] \tag{3}$$

$$t(\eta) = \frac{1}{\sqrt{1+\eta}}\left[(1+\eta)E\left(\sqrt{\frac{1-\eta}{1+\eta}}\right) - \eta K\left(\sqrt{\frac{1-\eta}{1+\eta}}\right)\right] \tag{4}$$

and for $\eta > 1$ then

$$v(\eta) = \sqrt{\frac{\eta}{2}}\left[2E\left(\sqrt{\eta-1}2\eta\right) - (\eta+1)K\left(\sqrt{\frac{\eta-1}{2\eta}}\right)\right] \tag{5}$$

$$t(\eta) = \sqrt{\frac{\eta}{2}}\left[2E\left(\sqrt{\eta-1}2\eta\right) - K\left(\sqrt{\eta-1}2\eta\right)\right] \tag{6}$$

where K and E are complete elliptic integrals of the first and second kind, respectively.

$$K(k) = \int_0^{\frac{\pi}{2}} \frac{dx}{\sqrt{1 - k^2 \sin^2 x}} \tag{7}$$

$$E(k) = \int_0^{\frac{\pi}{2}} \sqrt{1 - k^2 \sin^2 x}\,dx \tag{8}$$

The parameter β is known as the enhancement factor that has no physical significance, although it is associated with roughness, cleanliness and other properties of the surface material. The argument A is the effective area of the field emitter.

Seeding the emitters at three different peak surface electric field levels 10 MV/m, 20 MV/m, and 30 MV/m and recording the results suggest a trend that for a fixed emitter location, especially those near the point of maximum peak surface field, more emitted electrons penetrate the beam tube or bombard the surface of the beam tube at higher peak surface electric field, as shown in Fig. 10.

This phenomenon suggests that at lower gradients, the presence of a field emitter is more likely to produce an increased cryogenic loss because most of the energy is released to the cavity while at higher gradients, there is more concern on damages to the beam tube components and degradation of beam qualtiy due to the higher probability of emitted electrons being captured.
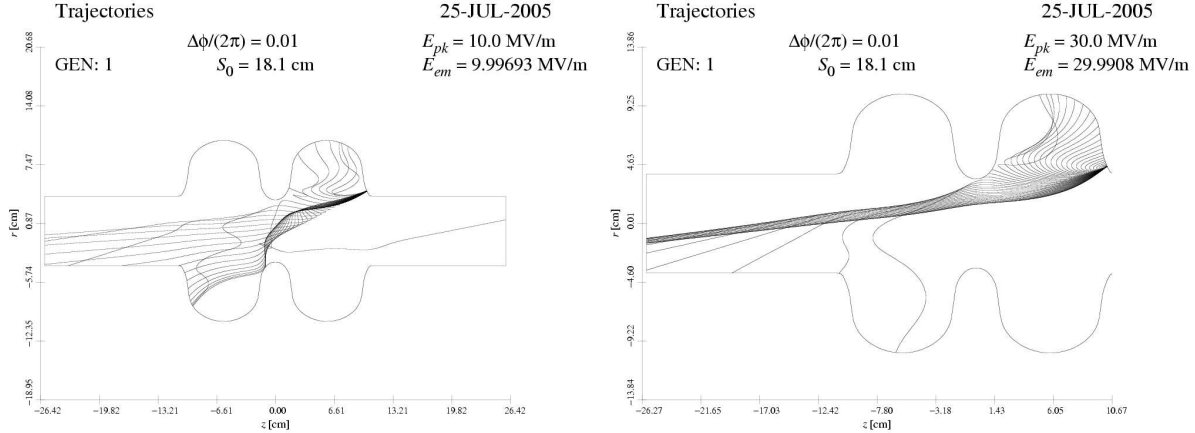
FIG. 10: Gradient Increase Effects — At a lower gradient, which corresponds to a lower peak surface electric field, the emitted electrons can hit a large region of the cavity as shown on the left. At higher gradients, at shown on the right, most trajectories penetrate the beam tube.

It is also noted that the secondary electrons generated by the bombardment of the beam tube tend to collimate and penetrate the beam tube. Typical emitted electrons, from an emitter with enhancement factor of 200 and area of 10^{-8}cm^2, have energies on the order of 10 keV to 1 MeV and bombard the beam tube at an angle, which allows them effectively generate secondary electrons.[8] The tendency for these secondary electrons to collimate into the beam tube can cause more damage, disturb the beam, and possibly contribute to "halo" and "dark current" phenomena.

The occurence of field emission induced multipacting was not established in this investigation, although plausible instances have been indentifed. In Fig. 11, a field emitter located at the upper half of a side iris can bombard the same iris on the lower half and yield secondary electrons that travel back to the vicinity of the emitter. More detailed phase and secondary emission curve analyses are required to establish this multipactor. However, this example illustrates potential field emission induced multipacting that merits further investigation.
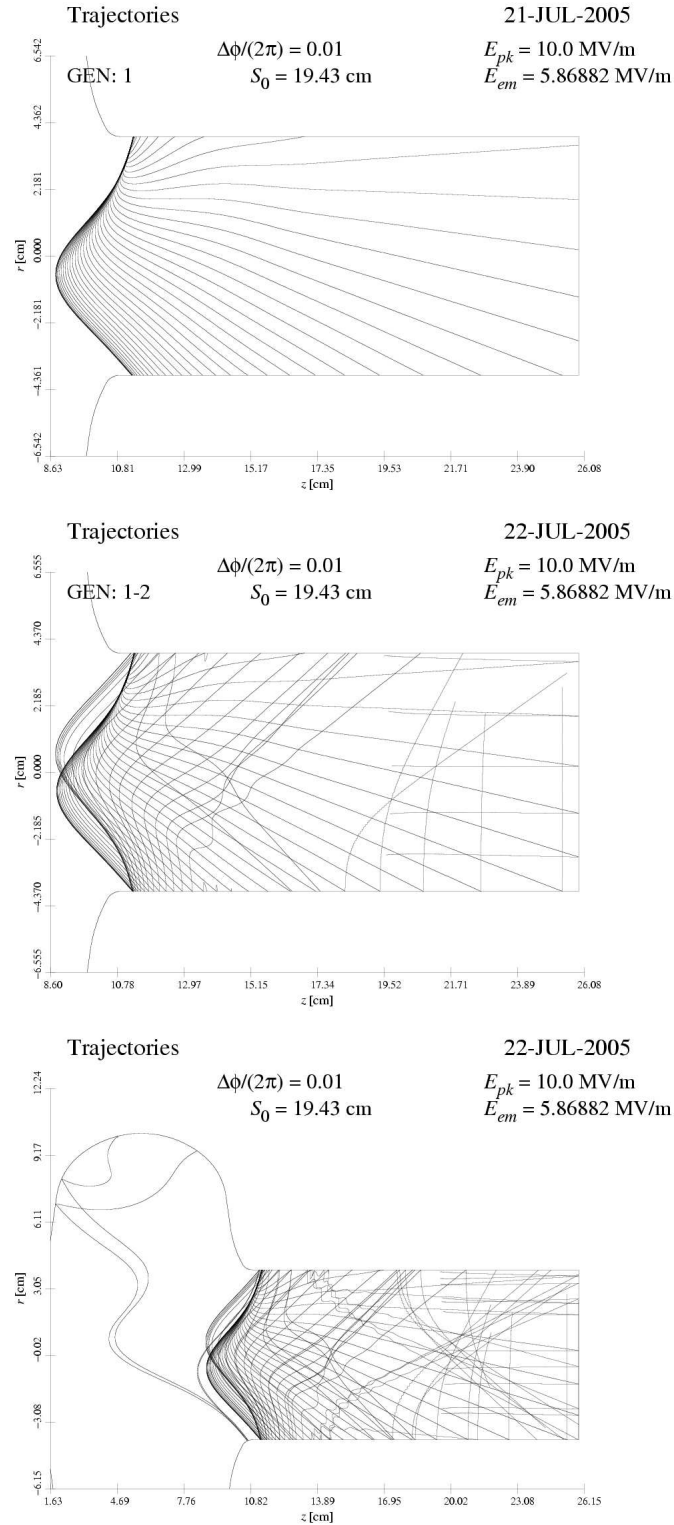
FIG. 11: Field Emission and Multipacting — The trajectories suggest that field emission induced multipacting may be possible. Top shows the trajectories of the field emitted electrons. The middle includes the secondary generation. The bottom includes all generations.

Another phenomenon of interest is a termporal focusing effect, or that a fixed emitter can continuously bombard points of close proximity over a significant fraction of the RF period, up to approximately 10 percent of an RF period, as illustrated in Fig. 12. However, a closer examination of the power density reveals that these focusing effects are usually of low power density because of the low current density as determined by the Fowler-Nordheim theory. However, cases, such as Fig. 13, have been identified where a focusing effect is accompanied by high power density, which is a dangerous combination because of the sigificant amount of energy that can be deposited over a small area.
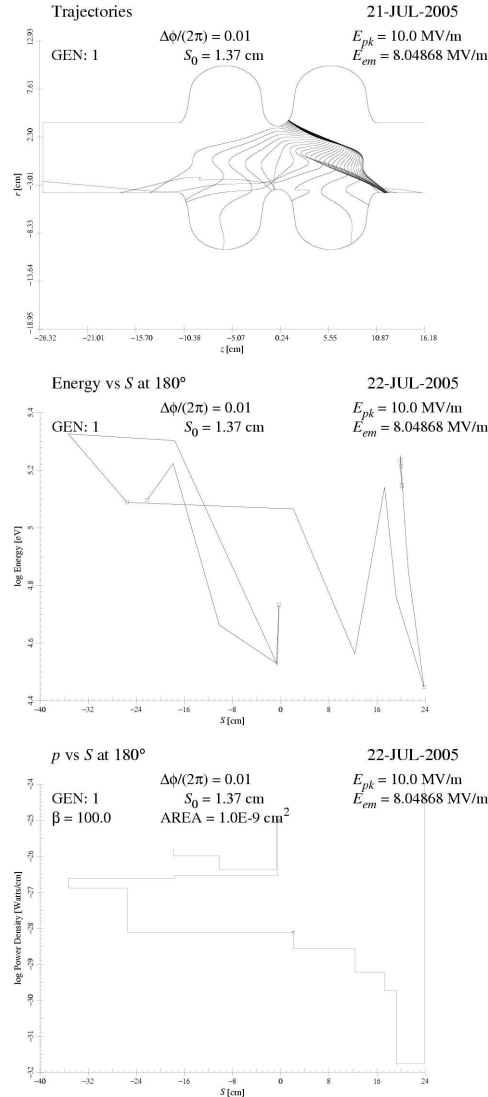

FIG. 12: Focusing Effect — The trajectories illistrated in the top diagram shows a focusing on an iris. The middle diagram shows that the energies of all the emitted electrons energies are within two order of magintude different. However, the bottom diagram shows that around 20 cm, the location of the iris, the power density is extremely low because of the low current density.

Trajectories   26-JUL-2005 p vs S at 0°   26-JUL-2005

$\Delta\phi/(2\pi) = 0.01$ $E_{pk} = 30.0$ MV/m $\Delta\phi/(2\pi) = 0.01$ $E_{pk} = 30.0$ MV/m
GEN: 1 $S_0 = 1.75$ cm $E_{em} = 24.587$ MV/m   GEN: 1 $S_0 = 1.75$ cm $E_{em} = 24.587$ MV/m
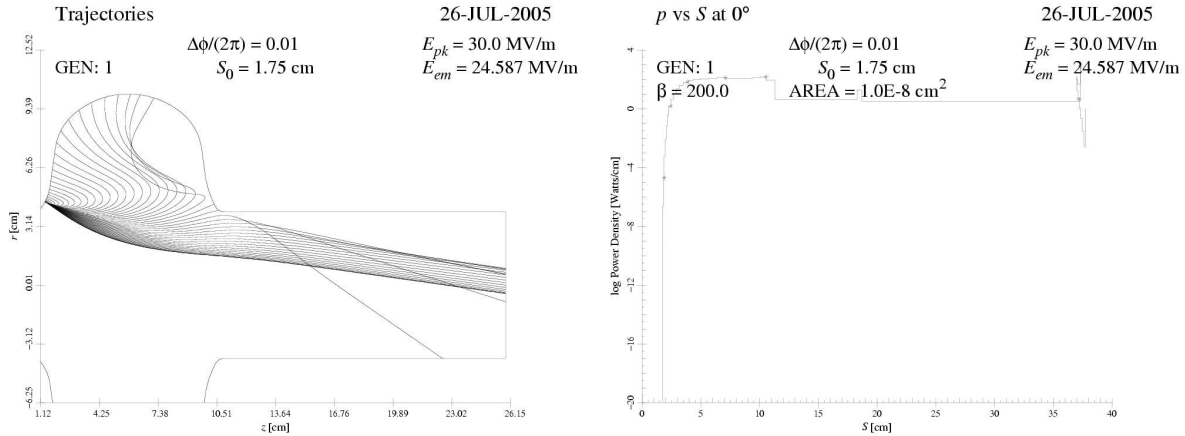 $\beta = 200.0$ AREA = 1.0E-8 cm^2

FIG. 13: High Power Focus — A noticeable focusing effect can be observed from the trajectory map on the left. The right shows that while the power density of focused trajectories, around 35 cm, are decreasing rapidly, most are only a couple of order of magnitudes below the other trajectories.

A noticeable characteristic of this cavity is that the energy of the field emitted electrons do not vary significantly with different peak surface electric field levels. Therefore, the total power output of an emitter in this cavity is dominated by the current output. This conjecture can be confirmed qualitatively by comparing Fig. 14 with the current density predictions of the Fowler-Nordheim theory in Fig. 15.[9] Fig. 14 also illustrates the profound impact of the enhancment factor to power output, or cryogenic loss.
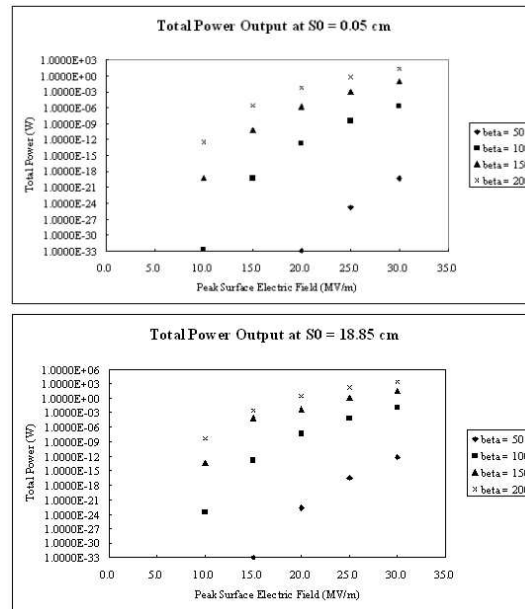

FIG. 14: Total Power Output — The two points were chosen for their high concentration of trajectories that bombard the cavity over multiple field levels. The effective emitter area chosen was 1×10^{-8}cm^2.

In order to evaluate the destructive capabilities of field emitters at different locations in this cavity, six emitter locations were chosen for detailed analysis: 1.75 cm and 18.1 cm away
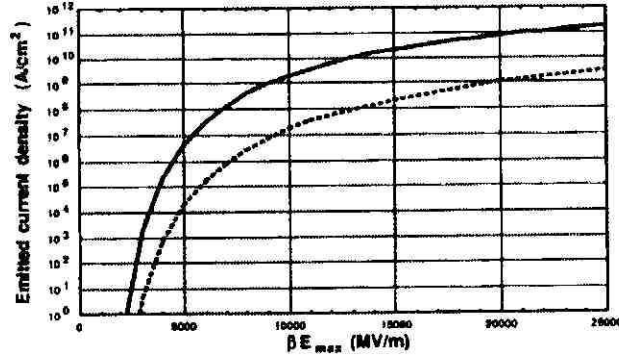
FIG. 15: Field Emission Current Density — Fowler-Nordheim theory predicts that effects of gradient and enhancement factor decrease when at high peak surface electric field or enhancement factor levels.

from the central plane on the cavity boundry are close to the maximum peak surface electric field in the central and side irises respectively; 17.8 cm and 18.9 cm are at 80 percent of the maximum peak surface electric field at the side iris; 1.3 cm marks a point that is close to the point of maximum peak electric field on the central iris yet most of the emitted electrons bombard the opposite side of the cavity; and 2.0 cm marks the edge of the seeded emitter positions for the central iris before reaching deep into the cavity region.

As shown in Fig. 16, the power output can vary significantly depending only emitter position. The extreme case of an emitter located at 18.1 cm, near the maximum peak surface electric field, has a total power output on the order of 10 kW because of the high field levels. Therefore, for this cavity geometry, 10 kW can be considered a reasonable upper bound for total power output of a typical unrestricted emitter. The actual power output may be lowered because of space charge effects that lower the current.
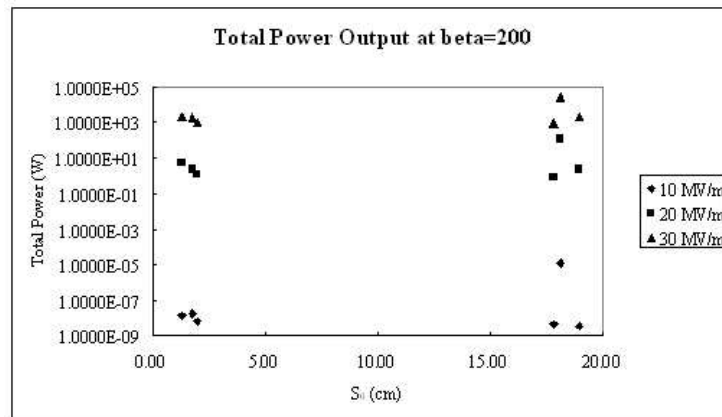

FIG. 16: Power Output Near Maximum Fields — The points chosen all have peak surface electric fields at least 80 percent of the maximum at that iris. Therefore, can be useful to find and set an upper bound for total power output for a single emitter. The effective emitter area chosen was $1 \times 10^{-8} \text{cm}^2$.

Acknowledgments

[1] V. Shemelin, H. Padamsee, and R. Geng, Nuclear Instruments and Methods in Physics Research A **496**, 1 (2003).

[2] R. Geng, H. Padamsee, A. Seaman, and V. Shemelin, Tech. Rep. 050608-03, Laboratory for Elementary-Particle Physics, Cornell University (2005).

[3] V. Baglin, J. Bojko, O. Gröbner, B. Henrist, N. Hilleret, C. Scheuerlein, and M. Taborelli, in *Proceedings of European Particle Accelerator Conference 2000* (European Physical Society Interdivisional Group on Accelerators, 2000).

[4] V. Shemelin, H. Padamsee, S. Belomestnykh, R. Geng, and M. Liepe, Tech. Rep. 030422-02, Laboratory for Elementary-Particle Physics, Cornell University (2003).

[5] S. Belomestnykh, Tech. Rep. 941208-13, Laboratory for Elementary-Particle Physics, Cornell University (1994).

[6] R. Ferraro, R. Kahn, W. Hartung, T. Flynn, and S. Belomestnykh, *Guide to Multipacting/Field Emission Simulation Software* (1996).

[7] E. Murphy and R. Good, Jr., Physical Review Series II **102**, 1464 (1956).

[8] J. Vaughan, IEEE Transactions on Electron Devices **36**, 1963 (1989).

[9] H. Padamsee, J. Knobloch, and T. Hays, *RF Superconductivity for accelerators* (John Wiley & Sons, 1998), p. 234, Wiley series in beam physics and accelerator technology.